Images of the Antiferromagnetic Structure of a NiO(100) Surface by Means of X-Ray Magnetic Linear Dichroism Spectromicroscopy

J. Stöhr,[1] A. Scholl,[2] T. J. Regan,[3] S. Anders,[2] J. Lüning,[1] M. R. Scheinfein,[4] H. A. Padmore,[2] and R. L. White[5]
[1]*IBM Research Division, Almaden Research Center, 650 Harry Road, San Jose, California 95120*
[2]*Advanced Light Source, Lawrence Berkeley National Laboratory, 1 Cyclotron Road, Berkeley, California 94720*
[3]*Department of Applied Physics, Stanford University, Stanford, California 94305*
[4]*Department of Physics and Astronomy, Arizona State University, Tempe, Arizona 85287-1504*
[5]*Materials Science and Engineering Department, Stanford University, Stanford, California 94305*
(Received 24 May 1999)

We present the first images of a surface showing clear antiferromagnetic contrast. The images were obtained for 10–80 nm thick NiO(100) films grown on Mg(100) by means of x-ray magnetic linear dichroism spectroscopy in conjunction with high resolution photoelectron emission microscopy. The surface sensitive images with a lateral resolution of better than 50 nm reveal surface line defects that exhibit antiferromagnetic order with a reduced Néel temperature (455 K) relative to the rest of the film surface and the bulk (523 K). Analysis of the temperature dependent images allows us to separate the spin and charge components of the linear dichroism effect.

PACS numbers: 75.70.–i, 75.30.Pd, 75.50.Ee, 78.20.Ls

In the last decade the ability to atomically engineer magnetic structures with reduced dimensions, such as thin film sandwiches and multilayers, has created new interest in the study of magnetism and magnetic materials [1]. While an abundance of work exists for ferromagnetic thin films, the study of antiferromagnetic thin films has been impeded by their magnetically compensated nature. The study of antiferromagnetic surfaces and interfaces has posed an even larger challenge because conventional optical, x-ray, and neutron techniques [2–4] are bulk sensitive. This limitation is overcome by the use of x-ray magnetic *linear* dichroism (XMLD) spectroscopy [5–9] carried out by means of surface sensitive electron yield detection [10,11]. In contrast to the x-ray magnetic *circular* dichroism (XMCD) technique [12–14] which directly measures the magnetic moment $\langle M \rangle$ through transfer of the x-ray angular momentum vector in the absorption process, XMLD spectroscopy measures the expectation value of the square of the magnetic moment, $\langle M^2 \rangle$, because linearly polarized photons have only axiality. In principle, XMCD can be used only for *unidirectional* magnetic systems, i.e., ferromagnets or ferrimagnets, while XMLD can be applied for all *uniaxial* magnetic systems, e.g., antiferromagnets, as well.

It has been suggested that, in principle, XMLD spectroscopy in conjunction with a photoelectron emission microscope (PEEM) should be capable of imaging the detailed antiferromagnetic domain structure of a surface or interface [10], similar to XMCD-PEEM spectromicroscopy of ferromagnets [15]. In comparison to other imaging techniques of antiferromagnetic domains such as neutron and x-ray diffraction topography [2,3,16], and optical [2,17] and nonlinear optical [18] techniques, XMLD-PEEM spectromicroscopy offers elemental specificity, surface sensitivity (~2 nm sampling depth [11]), and improved spatial resolution (~20 nm). In practice, however, it has been difficult to obtain reliable, meaningful antiferromagnetic images by XMLD microscopy as demonstrated by a recently published first attempt [19].

Here we report the first unambiguous surface images with antiferromagnetic contrast. They were obtained with XMLD microscopy for NiO(100) grown on MgO(100) and were made possible by a new spectromicroscopy facility at the Advanced Light Source (ALS) in Berkeley that combines a high flux-density soft x-ray beam line with a high spatial resolution PEEM [20]. The images reveal striking antiferromagnetic contrast which through atomic force microscopy images is linked to crystallographic line defects. From the temperature dependence of the surface integrated XMLD absorption *spectra* we find a NiO(100) surface Néel temperature that is indistinguishable from the bulk (523 K). Detailed analysis of the antiferromagnetic *images* reveals a different temperature dependence of the defect regions. This is attributed to a temperature dependent magnetic (spin) component of the XMLD contrast which vanishes at the reduced Néel temperature of the line defects (455 K), and a constant crystallographic (charge) component arising from a lower than cubic symmetry in the defects.

The 10–80 nm thick NiO(100) films on MgO(100) were grown by electron beam evaporation of elemental nickel in an activated oxygen atmosphere. Molecular oxygen was fed into the chamber (base pressure 4×10^{-8} torr) to a pressure of 2×10^{-5} torr, confined with a magnetic field, and activated with an electron cyclotron resonance microwave source. A typical growth rate was 0.3 Å/sec. Reflection high-energy electron diffraction patterns monitored during and after growth showed almost no change from the pattern of the MgO substrate, indicating that the NiO grew epitaxially in the desired MgO

 0031-9007/99/83(9)/1862(4)$15.00

rocksalt structure. High-angle symmetric and asymmetric x-ray diffraction scans confirmed the growth of single-phase epitaxial NiO(100). The NiO thickness was determined by small-angle x-ray diffraction. Bare NiO(100) surfaces were characterized with atomic force microscopy (AFM). The surfaces were generally smooth and composed of square growth regions of dimension 30–50 nm, as shown in Fig. 1. Linelike structures, arranged in a crisscross pattern, consisting of raised bars having cross sections 1–3 nm high and 30–1000 nm wide were also observed. Corresponding images of MgO(100) substrates, taken soon after polishing, suggested that imperfections in the substrate could be the source of the NiO surface features.

Spectromicroscopy studies were carried out using the PEEM2 facility on beam line 7.3.1.1 at the ALS [20]. Linearly polarized x rays are obtained by the use of an aperture that selects the central horizontal fan of radiation from a bending magnet source [10]. The sample is located in the focal plane of a slitless spherical grating monochromator and a horizontally focusing elliptical mirror with a 30 μm focal spot. The monochromatic photon flux density at the sample is $(3 \times 10^{12}$ photons/sec$)/(0.4$ eV$/30\ \mu\text{m}^2)$ at 800 eV and a ring current of 400 mA. The x rays are incident on the sample at an angle of 30° from the surface with the electric field vector $\vec{E}$ oriented parallel to the surface. The all electrostatic PEEM2 microscope collects low-energy, secondary photoelectrons from the sample. In order to avoid charging effects the NiO(100) sample was coated with a 2 nm Cu layer in the PEEM preparation chamber. The photoelectrons are imaged with magnification onto a phosphor screen which is read by a CCD camera. The spatial resolution of PEEM2 is limited by chromatic aberrations to 20 nm. The resolution for our studies was about 50 nm.

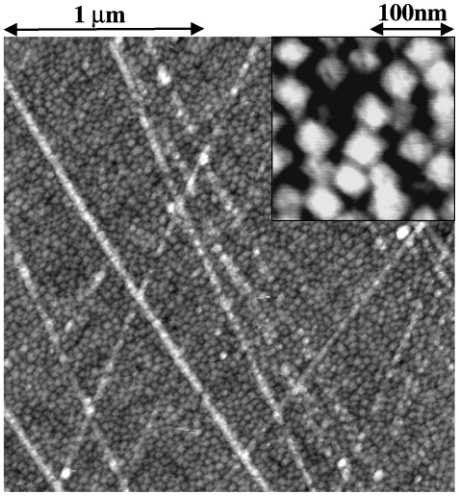

FIG. 1. Atomic force microscopy image of a 80 nm thick NiO(100) film grown on MgO(100). The inset shows a magnified part of the image.

The resonant absorption intensity of linearly polarized x rays may be written as [9,14]

$$I(\vartheta, \theta, T) = a + b(3\cos^2\vartheta - 1)\langle Q_{zz}\rangle + c(3\cos^2\theta - 1)\langle M^2\rangle_T + d\sum_{i,j}\langle \hat{s}_i \cdot \hat{s}_j\rangle_T . \quad (1)$$

The constant first term is independent of the x-ray polarization and the sample temperature T, the second term expresses the x-ray polarization dependence due to the presence of a quadrupole moment of the charge, $\langle Q_{zz}\rangle$, where ϑ is the angle of $\vec{E}$ with the crystallographic z axis, assuming higher than twofold symmetry about z. This term gives rise to the conventional linear dichroism effect in x-ray absorption [14]. The third term is responsible for the XMLD effect [9]. It depends on the x-ray polarization through the angle θ between $\vec{E}$ and the magnetic axis $\overleftrightarrow{A}$ and on temperature through $\langle M^2\rangle_T$. This term reflects the temperature dependence of the long range magnetic order and vanishes above the Néel temperature. Finally, the last term expresses the dependence on the short range magnetic order through the temperature dependent spin-spin correlation function $\langle \hat{s}_i \cdot \hat{s}_j\rangle_T$ [21].

In NiO the charge-only linear dichroism effect vanishes because of cubic symmetry ($\langle Q_{zz}\rangle = 0$) [14,22]. However, the alignment of the Ni spins along the antiferromagnetic axis $\overleftrightarrow{A}$ [17] leads to a pronounced XMLD effect whose angular and temperature dependence has been studied in detail for ultrathin NiO(100) films on MgO(100) [9,21]. In particular, the Ni L_2 edge exhibits two multiplet peaks of which the lower energy peak A is larger for $\vec{E} \perp \overleftrightarrow{A}$ and the higher energy peak B is larger for $\vec{E} \parallel \overleftrightarrow{A}$ [9]. The peak intensity ratio and its temperature dependence is dominated by the XMLD effect [9]. The smaller spin-spin correlation term was found to exhibit a similar temperature dependence as the $\langle M^2\rangle_T$ term [9,21]. The L_2 multiplet peak intensity ratio can therefore be used as spectroscopic contrast when imaging the magnetic configuration of the antiferromagnetically ordered NiO surface [10,19].

Figure 2 shows an antiferromagnetic image with a 40 μm field of view for a 10 nm thick NiO(100) film. The image was generated by dividing an image acquired at 871.5 eV, peak B, by one recorded at 870.3 eV, peak A. This procedure eliminates topographical and produces antiferromagnetic contrast. The image exhibits straight bright lines or stripes with typical widths between 400 and 2000 nm on a darker background. Such features are observed at other locations on the same sample and on other samples with different NiO thicknesses in the 10–80 nm range. The lines are several 100 μm long, and the fact that similar structures are also observed by AFM indicates that the lines in our image are correlated with the structure of the surface. However, the contrast in Fig. 2 is of antiferromagnetic and not of topographic nature.

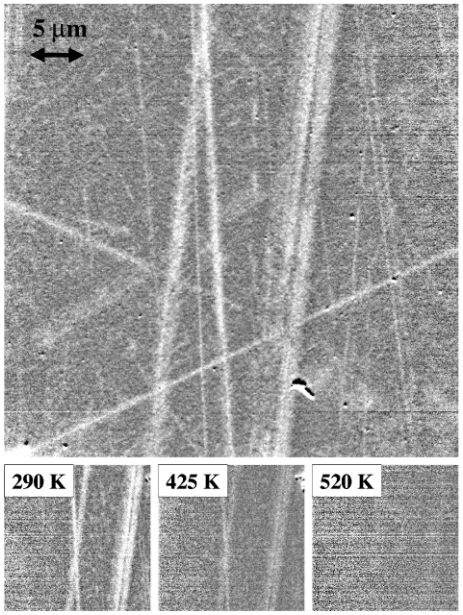

FIG. 2. XMLD antiferromagnetic image of a 10 nm thick NiO(100) film on MgO(100) recorded at room temperature, and the temperature dependence of a region within the image.

This is demonstrated by the temperature dependence of the image shown in Fig. 2. Here we show three images recorded at 290, 425, and 520 K, respectively. Clearly, the contrast disappears gradually as the Néel temperature of the film is approached. The temperature dependence is reversible and the XMLD contrast is fully restored upon returning to room temperature (see Fig. 4 below). This indicates that the linelike antiferromagnetic regions are pinned by the surface structure of the film.

Figure 3 shows temperature dependent absorption spectra obtained with PEEM from a large region of ~ 20 μm diameter, dominated by dark areas. The ratio of peak A (870.3 eV) and peak B (871.5 eV) intensities is plotted versus temperature in Fig. 3. At room temperature, peak A is larger than peak B indicating, on average, a preferred orientation of $\overleftrightarrow{A}$ perpendicular to the surface [9]. At higher temperatures the peak ratio decreases to 1.055 at $T = 520$ K, the same value found by Alders above the Néel temperature for thinner NiO films [9]. The solid line is a scaled superimposed curve using a $\langle M \rangle_T^2$ mean field theory [23] with the bulk value of T_N. Thus the disappearance of magnetism goes hand in hand with the reduction in image contrast.

We always observe bright stripes on a dark background when the sample is rotated about the surface normal. The stripes therefore do not correspond to azimuthally oriented antiferromagnetic domains. Close inspection of our XMLD images reveals a superstructure of light speckles which we believe to originate from the true antiferromagnetic domains. Their size is probably comparable to the square growth regions shown in the inset of Fig. 1 ($\leq$50 nm) which is at our resolution limit. A bright

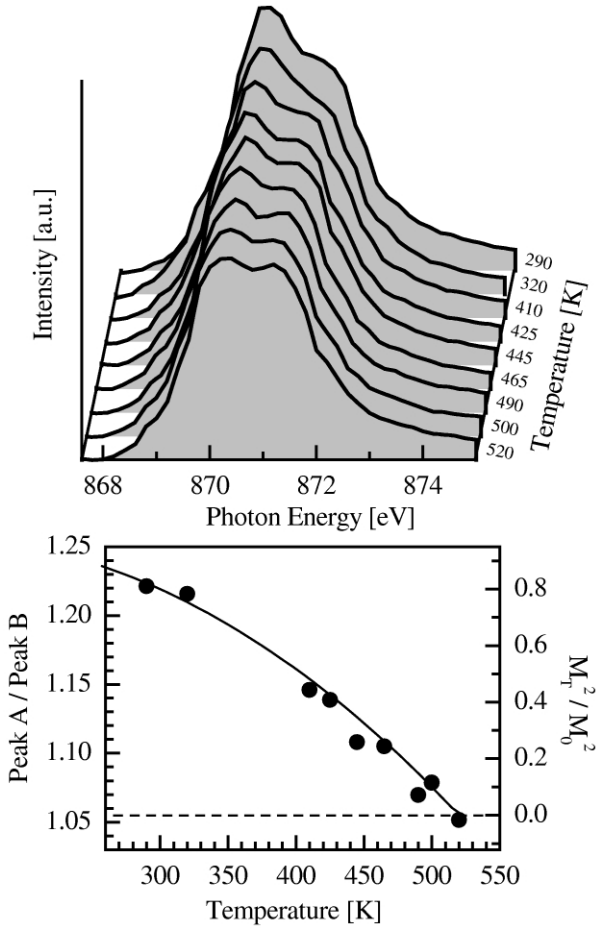

FIG. 3. Ni L_2-edge fine structure as a function of temperature for 10 nm NiO(100)/MgO(100). The spectra were obtained by averaging over a 20 μm diameter area of the sample, dominated by "dark" regions in the corresponding image. At the bottom we show the temperature dependence of the peak A (870.3 eV) to peak B (871.5 eV) intensity ratio. The solid line is a superimposed theory curve as discussed in the text.

area in the XMLD contrast image corresponds to an increased intensity of peak B relative to peak A. The stripes may thus be caused by a more in-plane orientation of $\overleftrightarrow{A}$ or, in accordance with Fig. 3, by a reduced value of $\langle M^2 \rangle$ associated with individual or an agglomeration of surface defect lines.

We can quantify the temperature dependent antiferromagnetic contrast in the XMLD images by direct comparison of the intensity of the stripes and the intensity of the darker areas. Figure 4 shows consecutive temperature dependent line profiles through the same image. We also show a temperature dependent plot of the line contrast defined as the difference of the line intensity (area) and the background intensity, normalized to the background intensity. This curve therefore reflects the true line defect signal, with any underlying nondefect background subtracted out. The signal shows a characteristic $\langle M \rangle_T^2$ temperature dependence with a reduced Néel temperature $T_N = 455 \pm 10$ K, indicated by the solid line

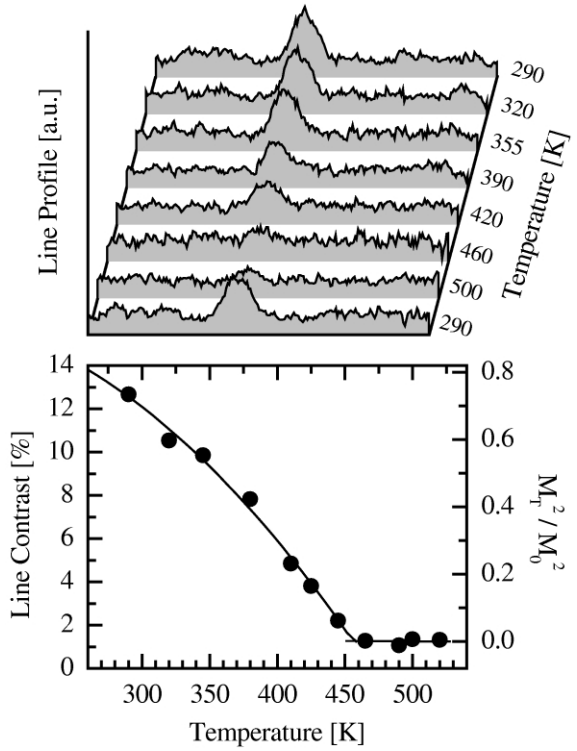

FIG. 4. Line scans across antiferromagnetic images of a 10 nm NiO(100)/MgO(100) sample at various temperatures. The peaks in the line scans are due to a "white" line in Fig. 2 and the peak intensity reflects the contrast. At the bottom we show the temperature dependence of the white line contrast and a theory curve (solid line) as discussed in the text.

theory curve [23]. This is attributed to a finite size effect [9] associated with the reduced dimension of the line defects. At higher temperatures the signal remains constant at a small but finite value. We attribute this to a temperature independent crystallographic (charge) contribution to the linear dichroism signal, i.e., a finite $\langle Q_{zz} \rangle$ term in Eq. (1), caused by a crystallographic distortion in the surface line defects.

The present study demonstrates the use of XMLD spectromicroscopy for obtaining detailed mesoscopic information on the antiferromagnetic structure of epitaxial thin films and their surfaces. More generally, it is clear that the technique can be extended to the study of polycrystalline surfaces and to interfaces between thin films.

This work was supported by the Director, Office of Basic Energy Sciences, of the U.S. Department of Energy under Contract No. DE-AC03-76SF00098. T. J. R. acknowledges the support of Stanford's Center for Materials Research and of IDEMA, and thanks M. R. Beasley's group for use of, and assistance with, their MBE chamber.

[1] J. B. Kortright, D. D. Awschalom, J. Stöhr, S. D. Bader, Y. U. Idzerda, S. S. P. Parkin, I. K. Schuller, and H.-C. Siegmann, J. Magn. Magn. Mater. (to be published); http://www-als.lbl.gov/als/workshops/scidirect/.

[2] W. L. Roth, J. Appl. Phys. **31**, 2000 (1960).

[3] J. Baruchel, Physica (Amsterdam) **192B**, 79 (1993).

[4] J. A. Borchers, R. W. Erwin, S. D. Berry, D. M. Lind, J. F. Ankner, E. Lochner, K. A. Shaw, and D. Hilton, Phys. Rev. B **51**, 8276 (1995).

[5] B. T. Thole, G. van der Laan, and G. A. Sawatzky, Phys. Rev. Lett. **55**, 2086 (1985).

[6] G. van der Laan, B. T. Thole, G. A. Sawatzky, J. B. Goedkoop, J. C. Fuggle, J.-M. Esteva, R. Karnatak, J. P. Remeika, and H. A. Dabkowska, Phys. Rev. B **34**, 6529 (1986).

[7] P. Carra, H. König, B. T. Thole, and M. Altarelli, Physica (Amsterdam) **192B**, 182 (1993).

[8] P. Kuiper, B. G. Searle, P. Rudolf, L. H. Tjeng, and C. T. Chen, Phys. Rev. Lett. **70**, 1549 (1993).

[9] D. Alders, L. H. Tjeng, F. C. Voogt, T. Hibma, G. A. Sawatzky, C. T. Chen, J. Vogel, M. Sacchi, and S. Iacobucci, Phys. Rev. B **57**, 11 623 (1998).

[10] J. Stöhr, H. A. Padmore, S. Anders, T. Stammler, and M. R. Scheinfein, Surf. Rev. Lett. **5**, 1297 (1998).

[11] R. Nakajima, J. Stöhr, and I. Idzerda, Phys. Rev. B **59**, 6421 (1999).

[12] G. Schütz, W. Wagner, W. Wilhelm, P. Kienle, R. Zeller, R. Frahm, and G. Materlik, Phys. Rev. Lett. **58**, 737 (1987).

[13] C. T. Chen, F. Sette, Y. Ma, and S. Modesti, Phys. Rev. B **42**, 7262 (1990).

[14] J. Stöhr, J. Electron Spectrosc. Relat. Phenom. **75**, 253 (1995).

[15] J. Stöhr, Y. Wu, B. D. Hermsmeier, M. G. Samant, G. R. Harp, S. Koranda, D. Dunham, and B. P. Tonner, Science **259**, 658 (1993).

[16] T. Yamada, S. Saito, and Y. Shimomura, J. Phys. Soc. Jpn. **21**, 672 (1966).

[17] S. Saito, M. Miura, and K. Kurosawa, J. Phys. C **13**, 1513 (1980).

[18] M. Fiebig, D. Frölich, S. Leute, and R. V. Pisarev, Appl. Phys. B **66**, 265 (1998).

[19] D. Spanke, V. Solinus, D. Knabben, F. U. Hillebrecht, F. Ciccacci, L. Gregoratti, and M. Marsi, Phys. Rev. B **58**, 5201 (1998).

[20] S. Anders, H. A. Padmore, R. M. Duarte, T. Renner, T. Stammler, A. Scholl, M. R. Scheinfein, J. Stöhr, L. Séve, and B. Sinkovic, Rev. Sci. Instrum. (to be published).

[21] D. Alders, J. Vogel, C. Levelut, S. D. Peacor, T. Hibma, M. Sacchi, L. H. Tjeng, C. T. Chen, G. van der Laan, B. T. Thole, and G. A. Sawatzky, Europhys. Lett. **32**, 259 (1995).

[22] The antiferromagnetic order results in a slight rhombohedral deformation in NiO [2] but the resulting $\langle Q_{zz} \rangle$ term is negligibly small.

[23] In general, $\langle M^2 \rangle_T = \langle M \rangle_T^2 + kT\chi(T)$, where $\chi(T)$ is the temperature dependent susceptibility (see, e.g., Chap. 2 in J. J. Binney, N. J. Dowrick, A. J. Fisher, and M. E. J. Newman, *The Theory of Critical Phenomena, An Introduction to the Renormalization Group* (Oxford University Press, New York, 1992). For an antiferromagnet $\langle M \rangle_T^2 \gg kT\chi(T)$ so that approximately $\langle M^2 \rangle_T = \langle M \rangle_T^2$. In Figs. 3 and 4 we have used the molecular field expression for $\langle M \rangle$ with $J = S = 1$, appropriate for the $3d^8$, ${}^3A_{2g}$ electronic ground state of NiO.